

Power Spectral Distribution of the BL Lacertae Object S5 0716+714

G.R. Mocanu, A. Marcu*

Abstract

Observational data in the BVRI bands of the variable BL Lacertae Object S5 0716+714 is discussed from the point of view of its Power Spectral Distribution (PSD). A model of the type $P(f) = \beta f^{-1} \left[1 + \left(\frac{f}{\delta} \right)^{\alpha-1} \right]^{-1} + \gamma$ is fitted to the data for four null hypothesis and the Bayesian p parameter for the fits is calculated. Spectral slopes with values ranging from 1.083 to 2.65 are obtained, with medium values for each band of $\overline{\alpha}_B = 2.028$, $\overline{\alpha}_V = 1.809$, $\overline{\alpha}_R = 1.932$ and $\overline{\alpha}_I = 1.54$ respectively. These values confirm conclusions of previous studies, namely that the source is turbulent. Two disk models, the standard prescription of the Shakura-Sunyaev disk and magnetized disks exhibiting MagnetoRotational Instability, were discussed. We found that it is unlikely that they explain this set of observational data.

keywordsturbulence; magnetic fields; accretion, accretion disks

1 Introduction

Extensive observational and theoretical efforts have been made in order to explain IntraDay Variability (IDV) in some classes of Active Galactic Nuclei (AGN). While variations in luminosity on scales of an year or more may be explained through processes usually associated with gravitationally supported Keplerian disks, the significant variations that occur on a timescale of less than a day are yet unexplained. There is almost an unanimous consent that explaining variations on all timescales is equivalent to proposing a robust angular momentum transport mechanism.

The object BL Lac S5 0716+714 was observed in numerous campaigns and in different wavelengths and is one of the most manifestly variable source in the AGN class (Wagner & Witzel 1995; Wagner et al. 1996; Qian, Tao & Fan 2002; Raiteri et al. 2003; Villata et al. 2008; Poon, Fan & Fu 2009; Chandra et al. 2011; Carini, Walters & Hopper 2011). Flares have been seen in all wavelengths (Wagner & Witzel 1995; Poon et al. 2009) and close IDV correlations between radio (at 6 cm wavelength) and optical (at 650 nm wavelength) have been reported (Wagner et al. 1996; Wagner et al. 1990; Quirrenbach et al. 1991). Krichbaum et al. (2002) discuss 15 years of observations for 40 sources and report the first detection of mm band IDV for S5 0716+714. We

*Corresponding author: alexandru.marcu@phys.ubbcluj.ro

emphasize on the flaring character, as no or little evidence for periodicity has been found. Qian (1995) reported that behavior changed from quasi periodic daily to less periodic weakly oscillations and Quirrenbach et al. (1991) report transitions from one dominant IDV scale to another. Krichbaum et al. (2002) find that above 8GHz the variability index increases with frequency. Qian et al. (2006) report this object in a study of IDV sources with very high polarizations. This indicates the presence of uniform background magnetic fields in the source.

When such a wealth of observational data is at hand, one may use it to discriminate between theoretical models (as e.g. Kraus et al. 1999). Quirrenbach et. al. (1992) comment that the correlated variations in simultaneous optical and radio variability cannot be explained by the action/interaction with the InterStellar Medium (ISM). Qian et al. (1996a;1996b) comment that shock propagating in an oscillatory jet might explain IDV and correlation between radio and optical IDV. Kirk & Mastichiadis (1992) propose models based on injection and acceleration of particles. Begelman, Rees & Sikora (1994) refines the relativistic jet model to explain the high brightness temperature theoretically associated to IDV. The model successfully reproduces the observed spectral index variations.

Chandra et al. (2011) discuss variability in optical BVRI bands during a 5 day monitoring campaign in March 2010. They present light curves and calculate variation rates. The fast variations and the high amplitudes in magnitude are difficult to explain through accretion disk models. If variation in the Doppler factor is allowed, the shock in jet framework might explain the bluer when brighter behavior, but it cannot explain the microvariability (i.e. variability on timescales of a few tens of minutes).

Carini et al. (2011) report B and I bands microvariability for a 5 night observation campaign in March 2003. They perform light curve analysis, timescale analysis, color analysis, structure function analysis and cross correlation analysis. They firmly reject the hypothesis that the observed spectra might arise following electron cooling. Their conclusion is that the observed microvariability is the result of a fractional noise process, i.e. the source of the variations is a turbulent process.

Azarnia, Webb & Pollock (2005) analyze a set of 10 nonconsecutive R band light curves by using the Discrete Fourier Transform in order to obtain the possible noise characteristics of the time series. The results they obtained led them to speculate that microvariability is the result of complex turbulent relativistic plasma process.

A very interesting type of IDV analysis is based on the calculation of the fractal dimension of the light curves (Leung et al. 2011b). The fractal dimension of the R-band observations indicates an almost pure "Brownian noise" (random walk) spectrum.

The purpose of this paper is to discuss the observational data first presented in Poon et al. (2009) from the point of view of its PSD. After presenting (Section 2) the observational data, a detailed PSD analysis of the variability is performed (Section 3). An attempt is made to fit two accretion disk models to the data (Section 4).

2 Observational data

The data we consider has been recorded in the optical band (more precisely, the BVRI bands) during October and December 2008 and February 2009. These sets of data

and the observational technical characteristics have been thoroughly analyzed and discussed in Poon et al. (2009). There are compelling arguments that the source is variable in the BVRI band and that the flares at different wavelengths are due to the same generating mechanism.

The analysis in Poon et al. (2009) includes the spectral changes this source exhibits, i.e. the way in which the amplitude changes as a function of wavelength, which is equivalent to the Spectral Energy Distribution (SED). We wish to continue their work by introducing Power Spectral Distribution (PSD) analysis in all available wavelengths.

The observational data is presented in Table 1, where the columns have the following meaning

1. identification code for each band and each Julian Day of observations (i.e. R5 means "about data taken in the R band in the fifth date");
2. the actual Julian Date. It may be that some observations were made from 2454865.99 to 2454866.4 so we considered them as being part of the same day and included them in the analysis as such;
3. band, from B (blue, $\lambda_B = 440nm$), R (red, $\lambda_R = 630nm$), V (visible, $\lambda_V = 550nm$), I (infrared, $\lambda_I = 900nm$);
4. amplitude of variability for each day and for that specific band (Poon et al. 2009), calculated here in units of σ

$$A = \frac{\sqrt{(A_{max} - A_{min})^2 - 2\sigma^2}}{\sigma}, \quad (1)$$

where σ will be given below;

5. number N of data points in that Julian Day (JD) and for that specific band;
6. \overline{m} , the medium magnitude measured that day
 $\overline{m} = \frac{\sum_{i=1}^N m_i}{N}$, where m_i stands for the magnitude at one point, $i = \overline{1, N}$;
7. root mean square deviation error σ calculated as $N\sigma = \sqrt{\sum_{i=1}^N (m_i^2 - \overline{m}^2)}$ for each day and in that specific band.

3 PSD Analysis

From the light curves (Poon et al. 2009) and the values of the variability amplitudes (the A values in Table 1) it is obvious that this BL Lac object presents microvariability in the BVRI bands. Our purpose is to determine the slope of the power spectrum of the variations. To this end, the *software R* and the *bayes.R* script are used, designed to detect periodic signals in red noise (Vaughan 2010). Periodicity is not expected, but the software is useful in obtaining fits of the slope of the power spectrum.

We will do this for each day of observations. The theoretical working models used by the .R routine (i.e. the available null hypotheses) are power law plus constant:

$$H_0 : S(f) = \beta f^{-\alpha} + \gamma, \quad (2)$$

bending power law plus constant:

$$H_1 : S(f) = \beta f^{-1} \left[1 + \left(\frac{f}{\delta} \right)^{\alpha-1} \right]^{-1} + \gamma, \quad (3)$$

power law:

$$H_2 : S(f) = \beta f^{-\alpha}, \quad (4)$$

and bending power law:

$$H_3 : S(f) = \beta f^{-1} \left[1 + \left(\frac{f}{\delta} \right)^{\alpha-1} \right]^{-1}. \quad (5)$$

After running the script for all the days and in each band, Table 2 was obtained, where the columns have the following significance

1. observation day, as defined in Table 1;
2. model used, i.e. one of the four available null hypotheses H_i (Eq. 2-5);
3. values of parameter $\theta_1 = \alpha$ (the standard deviation is given between the square brackets);
4. values of parameter $\theta_2 = \ln \beta$ (the standard deviation is given between the square brackets);
5. values of parameter $\theta_3 = \ln \gamma$ (the standard deviation is given between the square brackets). For the H_2 hypothesis there is no third parameter and this was denoted by a – symbol in the appropriate place. When there is no entry for a H_i it means that for that specific case the software returned an error;
6. values of parameter $\theta_4 = \ln \delta$ (the standard deviation is given between the square brackets);
7. the (Bayesian) posterior predictive p-value is used for model checking and has the advantage of having no dependence on unknown parameters. It may be used to assess whether the data are consistent with being drawn from the model (Vaughan 2010). If the values of the statistics are very small it is unlikely that the proposed model could reproduce the data.

As an example of the fits, the time series for V3 (Fig. 1) and the power spectra fit for models H_0 (Fig. 2 left) and H_2 (Fig. 2 right) and models H_1 (Fig. 3 left) and H_3 (Fig. 3 right) are shown here.

Some comments are in order regarding the results of the PSD analysis. First, the bending power law null hypotheses (H_1 and H_3) fail to produce results in most of the

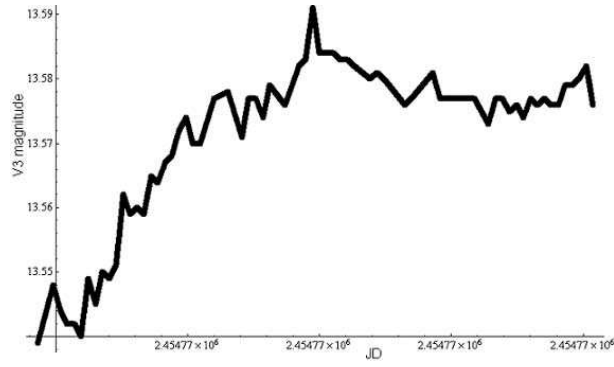


Figure 1: V3 time series.

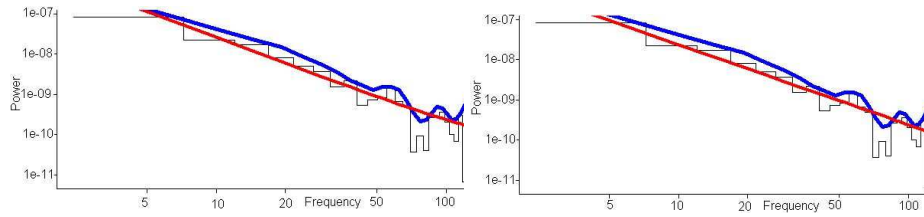


Figure 2: Fit (red curve) for model H_0 (left) and model H_2 (right) applied to the PSD (black curve) of the V3 time series.

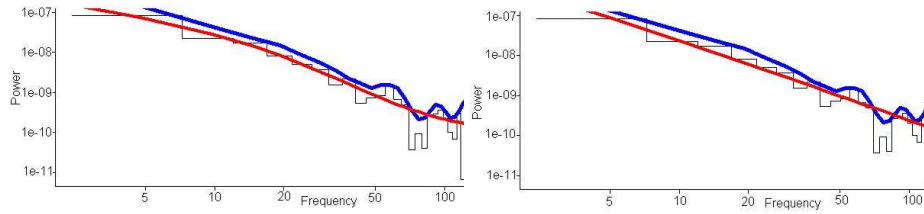


Figure 3: Fit (red curve) for model H_1 (left) and model H_3 (right) applied to the PSD (black curve) of the V3 time series.

cases. As seen in Table 2, for the cases where they do produce results, the standard mean deviations of the parameters are a lot bigger than for H_0 and H_2 .

Secondly, while the correct interpretation of the parameter set $\{\theta_2, \theta_3, \theta_4\}$ can provide valuable information, we will be interested in the PSD slope, i.e. $\theta_1 \equiv \alpha$.

Our interest follows from the known fact that the numerical values of the slopes of the PSD provide insight to the nature of the mechanism leading to the observed variability. In statistical analysis, if X is some fluctuating quantity, with mean μ and variance σ^2 , then a correlation function for quantity X is defined as

$$R(\tau) = \frac{\langle (X_s - \mu)(X_{s+\tau} - \mu) \rangle}{\sigma^2}. \quad (6)$$

where X_s is the values of X measured at time s and $\langle \rangle$ denotes averaging over all values s . The Power Spectral Distribution is defined based on the correlation function as

$$P(f) = \int_{-\infty}^{+\infty} R(\tau) e^{-i2\pi f\tau} d\tau \quad (7)$$

and it is straightforward to see its importance in terms of the "memory" of a given process. For example, if X is the B band magnitude of the disk, the slope of the PSD of a time series of X provides insight to the degree of correlation the underlying physical process has with itself. The system needs additional energy to fluctuate and this mechanism is historically best explained for Brownian motion, in which case the energy is thermal. Brownian motion produces a PSD $P(f) \sim f^{-2}$. Completely uncorrelated evolution of a system produces white noise, with a PSD $P(f) = f^0 = \text{const}$. It is then very interesting to try and explain how does a system evolve so as to produce a PSD for which α is neither 0 nor 2, as is the case for the time series discussed in this paper.

With this in mind, we now look at the θ_1 and p_B columns from Table 2. From each observation day we want to emphasize on the value of the PSD slope which satisfies both minimum standard mean deviation and maximum p_B criteria. However, this is not the case for all entries in the Table. In order to choose a value for the spectral slope (written in boldface in the Table) the following guidelines were used

1. we choose the values which clearly satisfy both the criteria and $p_B > 0.5$ (12 time series);
2. for cases when all p_B lie in the interval $[0.8, 1]$, but the minimum standard deviation is exhibited by the model with lower p_B , we favor the minimum standard mean deviation criterion (11 time series);
3. for cases when one p_B is above 0.5 and the rest are below, we favor the maximum p_B criterion (4 time series);
4. for cases when all p_B are below 0.5 we consider that the source does not behave like the null and do not use the obtained spectral slope for any further calculation. From our 41 time-series, 8 lie in this category (identification code written in bold);

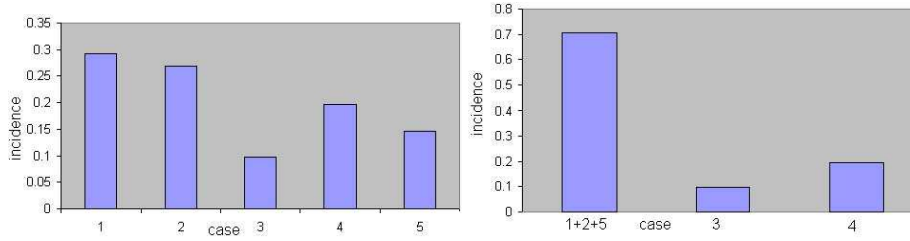


Figure 4: Left: Histogram of the number of time-series acceptably fitted by the null hypotheses of the .R software for the five cases discussed in the text. Right: Histogram for the occurrence of a valid power-law fit when cases 1, 2 and 5 are taken together.

5. for time series which fall in neither category we favor the maximum p_B criterion (6 time series). This would be the case of, e.g., V9.

With these considerations, the data provides slopes with values ranging from 1.083 to 2.65, with medium values for each band of $\bar{\alpha}_B = 2.028$, $\bar{\alpha}_V = 1.809$, $\bar{\alpha}_R = 1.932$ and $\bar{\alpha}_I = 1.54$ respectively.

It might prove to be an interesting exercise to do a histogram of these values (Fig. 4 left) to have a visual description of the validity of the power-law behaviour of the PSD. This is a pretty good result, showing that at least for this data set we may consider that the PSD behaviour of the source is well fitted by a power-law. This is a conclusion that becomes even more clearer if one views cases 1, 2 and 5 as one group and updates the histogram as in Fig. 4 right.

For the same object and a set of 10 nonconsecutive time series for the R band (2003 to 2005), Azarnia et al. (2005) obtain values for the spectral slope between -0.9 ± 0.122 and -1.393 ± 0.1005 . As emphasized by the authors, the $1/f$ results are not conclusive, but it is clear that the process noise is not white noise.

4 Theoretical models

Historically, there have been attempts to explain the variability through external effects e.g. RISS (Refractive Scintillation in the interstellar medium) (Wambsganss et al. 1989), microlensing (Wagner & Witzel 1995) or based on source morphology, e.g. a cluster of independently radiating objects (Krolik 1999, page 76). However, most of them fail because they do not predict the entire range of effects associated with variability.

A number of models study variability in the framework of efficient angular momentum transfer within the accretion disk, assuming that perturbations in this mechanism are responsible for the IDV. Mechanisms of angular momentum transfer may be conceptually divided in three different classes (Papaloizou & Lin 1995) based on the fundamental behaviour of the disturbance: hydromagnetic winds, waves in disks mechanism and thermal convection. None completely reproduces the observed characteristics of IDV.

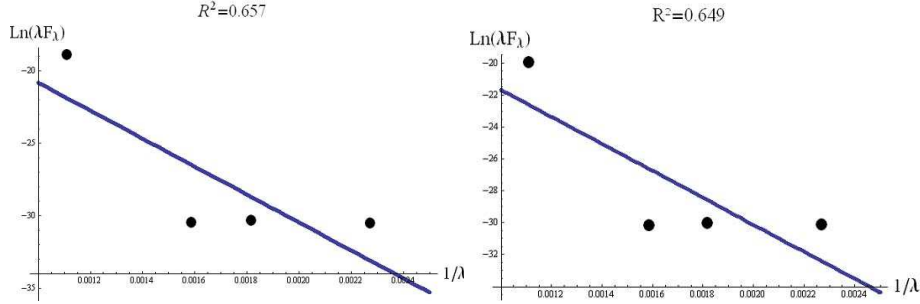


Figure 5: Plot of the logarithm of the medium λF_λ as a function of λ^{-1} , for the entire observational period (left) and for JD 2454866 (right). A fit of the type $\ln \lambda F_\lambda = a/\lambda + b$ was attempted, but it provides unsatisfactory results.

Through a series of papers (Mineshige, Ouchi & Nishimori 1994a; Mineshige, Takeuchi & Nishimori 1994b; Yonehara, Mineshige & Welsh 1997) there was an attempt to reproduce the PSD characteristics of IDV in a Self Organized Criticality framework. Realistic PSDs for the high energy (X-Ray) part of the spectrum may be obtained in this way.

Magneto Rotational Instability

The MagnetoRotational Instability (MRI, Balbus & Hawley 1991) is the most promising mechanism yet, its strength residing in the combination of differential rotation and the presence of an initially weak magnetic field. This approach has been systematically developed in the last few years to include theoretical and numerical discussion of various magnetic field configurations both in the linear and nonlinear regimes (Balbus & Hawley 1991, 1992a, 1992b; Hawley & Balbus 1991, 1992; Hawley, Gammie & Balbus 1995).

In order to qualitatively test the effect of MRI onset on the emergent spectrum, we propose the following reasoning. Theoretically, the emergent spectrum is proportional to the first power of the Reynolds-Maxwell stress tensor (Blaes 2002). The definition of this stress tensor, in the context adopted by us here is given in Balbus & Hawley (1998). Its value presents a dependency of the type $\exp\{-3/\lambda\}$. It is further assumed that λ , the wavelength of the disturbance, is also the observed wavelength. We calculated a medium flux for each wavelength for the entire observational campaign, and plotted $\ln(\lambda F_\lambda)$ as a function of the frequency corresponding to observed wavelength (Fig.5 left). The same algorithm was followed for a day of observations where data were available in all filters, i.e. for JD 2454866 (Fig. 5 right). In both cases, according to theory, we would expect a linear dependency, of the type $y \sim -3x$ which was not found. In fact, following this simple analysis, not even the linear character of the dependency is confirmed. An attempt to fit a function $y = ax + b$ to the data produced $R^2 = 0.657$ for the entire observational period and $R^2 = 0.649$ for JD 2454866.

The Shakura Sunyaev disk

The disk model presented by Shakura and Sunyaev in a series of papers (Shakura & Sunyaev 1973; 1976) starts from fundamental equations for geometrically thin disk accretion and perturbs these equations. They solve for the perturbations in surface density and height and express the total luminosity of the disk in terms of these perturbations. If the scale of perturbation is quantified by Ω ($\tau \propto 1/\Omega$), Ω evolves through a small strip of the parameter space (Shakura & Sunyaev (1976), Fig. 1), $\Omega/(\alpha_{SS}\omega) \in [0.02, 0.2]$, where α_{SS} is the Shakura-Sunyaev coefficient and $\omega = \sqrt{GM/R^3}$ is the Keplerian angular frequency.

If adimensional parameters $b = M/M_\odot$ and $d = R/R_g$ are used, the constraint from Shakura & Sunyaev (1976) may be re-written as

$$\frac{d^{3/2}b}{\tau\alpha_{SS}} \in [0.404, 4.047] \cdot 10^4. \quad (8)$$

For generally accepted numerical values for super-massive black holes, i.e. $d = 10$ and $b = 10^9$, and considering that the variability timescale is four hours, the constraint becomes

$$\alpha \in [0.18, 1.72] \cdot 10^{-2}. \quad (9)$$

Numerical simulations for the coefficient α place its value somewhere around 10^{-2} . The result in Eq.9 can be considered as a success of the model. It was already known that this mathematical formalism works but the problem still remains why it works, i.e. put the value of the coefficient of firm physical grounds.

However, based on recent data (Fan et al. 2011)¹ for this object, $\tau = 216s$ and $b \in [10^{7.68}, 10^{8.38}]$. If $d = 5$, then $\alpha_{SS} = 1.82$ for $b = 10^{7.38}$ and the value of α_{SS} grows as b and d grow (Eq. 8). It is then quite clear that the α_{SS} prescription of the standard disk model cannot explain the variability reported by Fan et al. (2011). With the benefit of this hindsight, we make the following argumentation, in order to obtain a "rule of thumb" to quickly asses whether or not a set of observational data may be explained by the standard disk model. Starting from Eq. 8 and considering $d \in [5, 10]$ a relation between τ , b and α_{SS} is obtained

$$\alpha_{SS} \in [0.0825, 2.475] \cdot \frac{b}{\tau} \cdot 10^{-4}. \quad (10)$$

If validity of the standard model is assumed, we must impose $\alpha_{SS} < 1$, which means that the ratio of the black hole mass to the variability time scale should be saturated at a finite value

$$\frac{b}{\tau} < [0.04, 1.212] \cdot 10^5. \quad (11)$$

This rule is very restrictive if one considers that typical values for b for AGNs are of the order $10^7 - 10^{10}$ and that IDV refers to timescales too small compared to those needed to satisfy relation 11.

¹We thank J. Fan for pointing this out.

Modelling IDV in a stochastic turbulence framework

A stochastic process is defined as a process where one or more of the variables of interest (called random variables) have some degree of uncertainty in their realization. At its base, stochastic modelling analyzes the evolution of some random variable and of its distribution function, with the aid of Langevin type equations and the Focker-Planck equation. Efforts to explain IDV in this framework are being developed. Leung et al. (2011a) take the random variable as the height of the disk and the stochastic component of the Langevin equation is set to mimic the interaction of the disk with a background cosmic environment.

If the random variable is taken to be the magnitude in one of the BVRI bands, three types of analysis of observational data, namely structure function analysis (Carini et al. 2011), fractal dimension analysis (Leung et al. 2011b) and DFT analysis (Azarnia et al. 2005) plus our own analysis establish that the source is turbulent, i.e. there is "intrinsic" noise superimposed on the deterministic behaviour of the source. The actual nature, onset and dissipation of turbulence is still a topic of discussion (Shakura & Sunyaev 1976; Balbus & Hawley 1998). At this point one can only speculate, but one educated guess is that the stochastic reconnection process proposed by Lazarian & Vishniac (1999) is an important part in producing of IDV. This process has proven successful in explaining fast and energetic in events over a large range of lengthscales.

5 Conclusions

The spectral slope and Bayesian confidence p-parameter for the BVRI bands observational data (Poon et al. 2009) were calculated. This was done for four null hypothesis available in the .R software (Vaughan 2010), Eqs. 2-5. The mean values for the spectral slope are $\overline{\alpha}_B = 2.028$, $\overline{\alpha}_V = 1.809$, $\overline{\alpha}_R = 1.932$ and $\overline{\alpha}_I = 1.54$. A histogram of the number of time-series which are well fitted by a PSD power-law is very encouraging, showing that the source presents power-law behavior in the BVRI bands. The values of the spectral coefficient confirm previous results which state that the source is noisy in a nontrivial way (Leung et al 2011b; Carini et al. 2011; Azarnia et al. 2005).

An attempt was made to explain the data in the context of two accretion disk models, the Shakura-Sunyaev disk and a magnetized disk exhibiting MRI. For standard AGN parameters the effective Shakura-Sunyaev parameter, α_{SS} , is within the theoretically correct interval, i.e. smaller than 1. However, if the new observational data of Fan et al. (2011) is taken into account, the hypothesis that IDV is produced within the disk is clearly not valid, since it would produce an α_{SS} with values well above 1. A naive rule of thumb to quickly assess whether or not IDV exhibited by some timeseries is produced within the standard prescription is derived, Eq. 11. The attempt to fit the data within an MRI framework was also unsuccessful, Fig. 5.

Acknowledgements

G.M. would like to thank T. Harko for valuable discussions on the topic of variability and suggestions regarding this work. This work was possible with the financial support of the Sectoral Operational Programme for Human Resources Development 2007-2013, co-financed by the European Social Fund, under the project number POS-DRU/107/1.5/S/76841 with the title "Modern Doctoral Studies: Internationalization and Interdisciplinarity". The authors thank the anonymous referee for valuable comments and suggestions.

References

- [1] Azarnia, G., Webb, J., Pollock, J.: 2005, I.A.P.P.P. Communications 101, 1
- [2] Balbus, S., Hawley, J.: 1991, ApJ 376, 214
- [3] Balbus, S., Hawley, J.: 1992a, ApJ 392, 662
- [4] Balbus, S., Hawley, J.: 1992b, ApJ 400, 610
- [5] Balbus, S., Hawley, J.: 1998, RevModPhys 70, 1
- [6] Begelman, M., Rees, J., Sikora, M.: 1994, ApJ 429, L57
- [7] Blaes, O.: 2002, Euro Summer School - NATO advanced study institute, 139
- [8] Balbus, S., Hawley, J.: 1992, ApJ 400, 610
- [9] Carini, M., Walter, R., Hopper, L.: 2011, ApJ 141, 49
- [10] Chandra, S., Baliyan, K., Ganesh, S., Joshi, U.: 2011, ApJ 731, 118
- [11] Fan, J.H., Tao, J., Qian, B.C., Liu, Y., Yang, J.H., Pi, F.P., Xu, W.: 2011, RAA 11, 1311
- [12] Hawley, J., Balbus, S.: 1991, ApJ 376, 223
- [13] Hawley, J., Balbus, S.: 1992, ApJ 400, 595
- [14] Hawley, J., Gammie, C., Balbus, S.: 1995, ApJ 440, 472
- [15] Kirk, J., Mastichiadis, A.: 1992, Nature 360, 135
- [16] Kraus, A., Quirrenbach, A., Lobanov, A., et al: 1999, AA 344, 807
- [17] Krichbaum, T., Kraus, A., Fuhrman, L., Cimo, G., Witzel, A.: 2002, PASA 19, 14
- [18] Krolik, J.: 1999, Active Galactiv Nuclei. From the central black hole to the galactic environment, Princeton new Jersey: Princeton University Press
- [19] Lazarian, A., Vishniac, E.: 1999, ApJ 517, 700
- [20] Leung, C., Wei, J., Harko, T., Kovacs, Z.: 2011a, J. Astrophys. Astr. 32, 189
- [21] Leung, C., Wei, J., Kong, A., Kovacs, Z., Harko, T.: 2011b, RAA 11, 1031L
- [22] Mineshige, S., Ouchi, N.B., Nishimori, H.: 1994, PASJ 46, 97
- [23] Mineshige, S., Takeuchi, N., Nishimori, H.: 1994, ApJ 435, L125
- [24] Papaloizou, J., Lin, D.: 1995, ANAA 33, 505
- [25] Poon, H., Fan, J., Fu, J.: 2009, ApJS 185, 511

- [26] Qian, B., Tao, J., Fan, J.: 2002, AJ 123, 678
- [27] Qian, S.: 1995, Chin.AA 19, 69
- [28] Qian, S., Krichbaum, T., Witzel, A., Zensus, J., Zhang, X.: 2006, Chin.AA 6, 530
- [29] Qian, S., Wegner, L., Witzel, A., Krichbaum, T.: 1996a, Chin.AA 20, 15
- [30] Qian, S., Witzel, A., Kraus, A., Krichbaum, T., Britzen, S.: 1996b, ASp Conf. Series 100, 55
- [31] Quirrenbach, A., Witzel, A., Kirchbauij, T.P., et al: 1992, AA 258, 279
- [32] Quirrenbach, A., Witzel, A., Wagner, S., et al: 1991, ApJ 372, L71
- [33] Raiteri, C., Villata, M., Tosti, G., et al: 2003, AA 402, 151
- [34] Shakura, N., Sunyaev, R.: 1973, AA 24, 337
- [35] Shakura, N., Sunyaev, R.: 1976, MNRAS 175, 623
- [36] Vaughan, S.: 2010, MNRAS 402, 307
- [37] Villata, M., Raiteri, C., Larionov, V., et al: 2008, AA 481, L79
- [38] Wagner, S., Sanchez-Pons, F., Quirrenbach, A., Witzel, A.: 1990, AA 235, L1
- [39] Wagner, S., Witzel, A.: 1995, ARAA 33, 163
- [40] Wagner, S., Witzel, A., Heidt, A., et al: 1996, AA 224, L9
- [41] Wambsganss, J., Schneider, P., Quirrenbach, A., Witzel, A.: 1989, AA 224, L9
- [42] Yonehara, A., Mineshige, S., Welsh, W.: 1997, ApJ 486, 388

	JD		A[σ]	N	\overline{m} [magn]	σ
B1	2454824	B	43.28191	107	14.30222	0.003395
B2	2454826	B	45.39896	127	14.25919	0.001805
B3	2454828	B	19.18941	37	14.55843	0.003118
B4	2454866- 2454867	B	55.58283	126	13.8741	0.003111
B5	2454871- 2454872	B	35.77494	103	14.24217	0.007821
B6	2454872- 2454873	B	35.76081	86	14.6071	0.00366
V1	2454765	V	27.03456	93	13.53289	0.007609
V2	2454766	V	26.14296	82	13.50011	0.006226
V3	2454767	V	57.34061	64	13.57052	0.000907
V4	2454770	V	30.20165	80	13.73929	0.004498
V5	2454824	V	49.68765	107	13.80678	0.002776
V6	2454825	V	32.8199	108	13.65370	0.003988
V7	2454826	V	51.5246	128	13.76498	0.001474
V8	2454828	V	38.47998	52	14.06906	0.001948
V9	2454829	V	51.44625	148	13.83567	0.00136
V10	2454830	V	46.83345	85	13.78665	0.00064
V11	2454865- 2454866	V	53.95782	178	13.77554	0.002001
V12	2454866- 2454867	V	51.84826	127	13.4035	0.002873
V13	2454871- 2454872	V	34.44135	103	13.75483	0.007485
V14	2454872- 2454873	V	35.6525	86	14.1083	0.003335
R1	2454765	R	26.80611	92	13.11834	0.006743
R2	2454766	R	27.18165	84	13.09189	0.005658
R3	2454767	R	25.38848	62	13.15161	0.001652
R4	2454770	R	27.59172	79	13.31928	0.00409
R5	2454824	R	49.72761	107	13.36121	0.002493
R6	2454825	R	37.45431	111	13.21392	0.003629
R7	2454826	R	46.4458	127	13.34012	0.001485
R8	2454828	R	22.699	51	13.61788	0.002462
R9	2454829	R	41.44746	148	13.40384	0.001591
R10	2454830	R	47.92965	85	13.35033	0.000667
R11	2454865- 2454866	R	55.61234	177	13.35199	0.002013
R12	2454866- 2454867	R	47.78895	110	12.99796	0.002845

R13	2454871- 2454872	R	32.6797	102	13.33697	0.007184
R14	2454872- 2454873	R	33.04623	85	13.63736	0.003144
I1	2454824	I	63.01641	107	0.05715	0.002475
I2	2454825	I	37.51954	109	-0.11376	0.003702
I3	2454826	I	48.21065	129	0.015481	0.001534
I4	2454828	I	29.17502	51	0.300137	0.002157
I5	2454830	I	44.49193	84	0.047845	0.000809
I6	2454866- 2454867	I	63.7564	125	1.357992	0.001129
I7	2454871- 2454872	I	32.23456	102	0.054029	0.005672

Table 1: Observational data, with $B \rightarrow 440nm$, $R \rightarrow 630nm$, $V \rightarrow 550nm$, $I \rightarrow 900nm$.

		θ_1	θ_2	θ_3	θ_4	p_B
B1	H_1	0.782 [1.415]	11.427 [21.173]	-19.091 [11.405]	-34.85 [14.401]	1
	H_2	1.821 [0.155]	-11.765 [0.633]	-	-	1
	H_3	1.923 [0.662]	-19.949 [24.702]	1.222 [11.639]	-	0.999
B2	H_0	2.517 [0.333]	-12.214 [0.962]	-22.583 [0.349]	-	0.501
	H_2	1.828 [0.116]	-13.802 [0.498]	-	-	0.193
B3	H_0	2.184 [0.557]	-12.081 [1.641]	-27.685 [7.306]	-	0.96
	H_2	1.877 [0.262]	-12.852 [1.02]	-	-	0.683
B4	H_0	2.15 [0.304]	-11.278 [0.902]	-22.029 [1.615]	-	1
	H_1	2.137 [0.588]	-9.011 [6.632]	-2.083 [10.563]	-21.828 [1.34]	0.999
	H_2	1.842 [0.124]	-12.058 [0.523]	-	-	0.945
B5	H_0	2.286 [0.412]	-9.341 [1.122]	-18.867 [0.871]	-	0.938
	H_1	3.637 [2.305]	-3.87 [17.143]	-5.56 [7.76]	-19.697 [1.701]	0.912
	H_2	1.654 [0.13]	-10.862 [0.523]	-	-	0.997
B6	H_0	2.639 [0.58]	-11.141 [1.273]	-19.78 [0.334]	-	0.914
	H_2	1.53 [0.143]	-13.228 [0.557]	-	-	0.397
V1	H_0	2.372 [0.389]	-8.82 [1.313]	-22.231 [3.229]	-	1
	H_2	1.964 [0.143]	-10.061 [0.664]	-	-	0.994
V2	H_0	2.271 [0.404]	-9.316 [1.328]	-20.777 [1.397]	-	1
	H_2	1.822 [0.158]	-10.622 [0.714]	-	-	1
V3	H_0	2.026 [0.243]	-12.837 [0.972]	-44.782 [15.266]	-	0.926
	H_1	3.195 [1.712]	4.575 [5.77]	-14.488 [2.021]	-28.615 [4.354]	0.947
	H_2	2.012 [0.212]	-12.857 [0.886]	-	-	0.857

	H_3	2.76 [2.059]	3.792 [76.601]	0.24 [25.477]	-	0.882
V4	H_0	2.28 [0.388]	-10.145 [1.278]	-25.1 [5.594]	-	1
	H_1	1.558 [0.896]	-0.124 [41.476]	-9.322 [7.371]	-22.437 [1.019]	1
	H_2	1.965 [0.158]	-11.067 [0.709]	-	-	1
V5	H_0	1.932 [0.341]	-11.664 [1.044]	-23.652 [5.714]	-	1
	H_1	3.583 [3.026]	-1.417 [4.747]	-9.868 [4.274]	-20.371 [0.567]	1
	H_2	1.59 [0.137]	-12.579 [0.556]	-	-	0.992
V6	H_0	3.218 [0.401]	-10.434 [0.935]	-22.473 [0.283]	-	0.409
	H_2	2.237 [0.116]	-12.347 [-0.488]	-	-	0.042
V7	H_0	2.76 [0.424]	-12.099 [1.024]	-22.186 [0.257]	-	0.48
	H_2	1.692 [0.106]	-14.297 [0.46]	-	-	0.014
V8	H_0	2.914 [1.388]	-11.22 [2.894]	-19.98 [0.946]	-	0.998
	H_2	1.083 [0.199]	-14.964 [0.789]	-	-	0.83
V9	H_0	2.331 [0.266]	-12.314 [0.842]	-22.683 [0.307]	-	0.923
	H_2	1.683 [0.103]	-14.01 [0.475]	-	-	0.537
V10	H_0	1.636 [0.633]	-15.595 [1.454]	-23.307 [2.94]	-	0.776
	H_2	1.06 [0.155]	-16.763 [0.599]	-	-	0.718
V11	H_0	1.788 [0.166]	-13.235 [0.618]	-28.954 [6.43]	-	0.536
	H_2	1.722 [0.097]	-13.423 [0.447]	-	-	0.661
V12	H_0	2.65 [0.377]	-10.146 [1.101]	-20.554 [0.27]	-	0.923
	H_1	3.167 [0.988]	-0.139 [2.438]	-9.634 [3.319]	-20.473 [0.225]	0.984
	H_2	1.664 [0.114]	-12.653 [0.478]	-	-	0.662
V13	H_0	1.816 [0.276]	-10.514 [0.829]	-25.257 [5.452]	-	0.952
	H_2	1.708 [0.145]	-10.75 [0.582]	-	-	0.969
V14	H_0	2.504 [0.434]	-11.444 [1.095]	-20.488 [0.507]	-	0.359
	H_2	1.665 [0.141]	-13.144 [0.55]	-	-	0.041
R1	H_0	2.299 [0.343]	-9.162 [1.192]	-22.296 [3.029]	-	1
	H_2	1.971 [0.143]	-10.151 [0.653]	-	-	0.994
R2	H_0	1.963 [0.169]	-10.265 [0.758]	-33.563 [4.956]	-	1
	H_2	1.957 [0.164]	-10.288 [0.735]	-	-	1
R3	H_0	2.548 [1.603]	-11.829 [4.261]	-68.786 [52.262]	-	0.999
	H_2	1.906 [0.228]	-13.515 [0.968]	-	-	1
	H_3	1.78 [2.459]	-1.949 [14.328]	-13.67 [6.54]	-	0.994
R4	H_0	2.287 [0.428]	-10.186 [1.397]	-22.434 [2.601]	-	1
	H_2	1.854 [0.158]	-11.444 [0.699]	-	-	0.999
R5	H_0	1.715 [0.217]	-12.345 [0.717]	-29.301 [9.384]	-	0.934
	H_1	1.988 [1.533]	-8.417 [18.501]	-9.563 [3.639]	-24.388 [3.974]	0.93
	H_2	1.654 [0.151]	-12.466 [0.621]	-	-	0.951
R6	H_0	2.413 [0.277]	-11.689 [0.76]	-24.214 [2.621]	-	0.876
	H_2	2.178 [0.121]	-12.165 [0.505]	-	-	0.256

R7	H_0	2.389 [0.318]	-12.693 [0.869]	-22.236 [0.323]	-	0.804
	H_2	1.671 [0.108]	-14.255 [0.465]	-	-	0.312
R8	H_0	2.767 [1.933]	-13.789 [4.617]	-24.024 [5.106]	-	0.929
	H_2	1.51 [0.241]	-13.792 [0.943]	-	-	0.859
R9	H_0	1.934 [0.274]	-13.187 [0.879]	-25.392 [3.993]	-	0.983
	H_2	1.666 [0.107]	-13.941 [0.492]	-	-	0.923
R10	H_0	2.668 [0.944]	-13.513 [1.909]	-21.319 [0.297]	-	0.606
	H_1	1.696 [1.723]	57.207 [119.484]	-84.994 [161.649]	-21.591 [1.058]	0.604
	H_2	1.107 [0.143]	-16.565 [0.56]	-	-	0.67
R11	H_0	1.724 [0.114]	-13.101 [0.512]	-54.669 [17.637]	-	0.28
	H_2	1.717 [0.107]	-13.122 [0.49]	-	-	0.311
R12	H_0	2.399 [0.364]	-11.009 [1.073]	-24.938 [6.496]	-	0.962
	H_1	2.567 [0.452]	-2.288 [2.48]	-7.474 [3.559]	-21.72 [0.511]	0.967
	H_2	2.006 [0.145]	-12.001 [0.585]	-	-	0.745
R13	H_0	1.881 [0.245]	-10.344 [0.76]	-25.802 [5.618]	-	0.995
	H_2	1.78 [0.144]	-10.606 [0.578]	-	-	0.979
R14	H_0	2.517 [0.397]	-11.687 [1.049]	-21.737 [0.678]	-	0.959
	H_2	1.944 [0.146]	-12.9 [0.574]	-	-	0.774
I1	H_0	1.364 [0.202]	-2.158 [0.727]	-20.594 [7.576]	-	0.991
	H_1	2.07 [1.577]	1.232 [4.893]	-1.496 [2.264]	-12.817 [3.63]	0.982
	H_2	1.333 [0.156]	-2.239 [0.64]	-	-	0.985
I2	H_0	2.361 [0.312]	-1.834 [0.893]	-11.504 [0.428]	-	0.282
	H_2	1.775 [0.119]	-3.099 [0.502]	-	-	0.258
I3	H_0	2.728 [0.416]	1.421 [1.06]	-7.975 [0.188]	-	0.361
	H_2	1.395 [0.094]	-1.406 [0.415]	-	-	0.033
I4	H_2	1.405 [0.244]	-6.419 [0.942]	-	-	0.747
I5	H_0	1.943 [0.979]	-3.732 [1.843]	-10.396 [1.627]	-	0.175
	H_1	3.144 [2.228]	-32.259 [374.247]	31.418 [278.444]	-8.946 [0.711]	0.19
	H_2	0.903 [0.156]	-5.634 [0.604]	-	-	0.151
I6	H_2	0.376 [0.167]	-13.277 [0.688]	-	-	0.622
	H_3	1.702 [2.878]	6.767 [4.691]	-10.319 [0.436]	-	0.949
I7	H_0	2.229 [0.323]	0.52 [0.92]	-8.81 [0.93]	-	0.863
	H_2	1.722 [0.133]	-0.625 [0.543]	-	-	0.952

Table 2: Results of spectral analysis.